INTERNATIONAL JOURNAL FOR NUMERICAL METHODS IN FLUIDS
Int. J. Numer. Meth. Fluids 2003; **43**:1391–1405 (DOI: 10.1002/fld.625)

A discontinuous Galerkin method/HLLC solver for the Euler equations

Malika Remaki[†,‡] and Wagdi G. Habashi[*,§,¶]

Computational Fluid Dynamics Laboratory, McGill University, 688 Sherbrooke Street West Montreal, QC, H3A 2S6, Canada

SUMMARY

This paper proposes a fully three-dimensional non-linear Euler methodology for solving aerodynamic and acoustic problems in the presence of strong shocks and rarefactions. It uses a discontinuous Galerkin method (DGM) within the element, and a Riemann solver (HLLC) at the boundaries to propagate rarefactions while preserving the entropy condition and capturing shocks with no spurious oscillations. This approach is thought to marry the best aspects of finite element and finite volume methods, achieving conservation while not requiring the solution of a large matrix. Examples in which shock and rarefaction waves are well captured are presented and the propagation of acoustic pulses is well demonstrated. Copyright © 2003 John Wiley & Sons, Ltd.

KEY WORDS: Non-linear problems; discontinuous Galerkin; finite element; finite volume; shocks; rarefactions; aerodynamics; acoustics; HLLC solver

1. INTRODUCTION

We present in this paper a 3D methodology for solving aerodynamic problems in the presence of strong shocks and rarefactions. It is proposed to use the discontinuous Galerkin method (DGM), introduced by Reed and Hill [1] for the neutron transport equations and subsequently generalized to fluid mechanics by Cockburn and Shu [2], and recently applied to the 2D Navier–Stokes equations by Bassi *et al.* [3]. Other authors applied this methodology to other physical applications such as electromagnetism, see References [4, 5]. Karniadakis and Sherwin [6] and Warburton [7], have developed a hierarchical tensor-type basis to get high-order schemes. A literature review can be found in Reference [8].

*Correspondence to: W. G. Habashi, Department of Mechanical Engineering, McGill University, 688 Sherbrooke Street West, 7th Floor, Montreal, Quebec, H3A 2S6, Canada.
†Research Associate, CFD Lab, McGill University.
‡E-mail: remaki@cfdlab.mcgill.ca
§Professor and Director of CFD Lab, McGill university.
¶E-mail: wagdi.habashi@mcgill.ca

Received 4 November 2002
Revised 2 July 2003

The DGM applies the Galerkin approach to each element via a local basis function, but solves the governing equations in a finite element space of discontinuous functions. The resulting equations remain local to the generating element and the only matrix inversion required is that of a local mass matrix, which can be diagonalized via an appropriate basis function set.

The local integration by parts then yields the trace of the flux vector on the boundary of each element. A suitable Riemann solver, chosen here to be the HLLC solver [9], can be used to define these fluxes. The choice of the numerical fluxes is very important in the presence of shocks and rarefactions and since the exact Riemann solver would be very expensive, for non-linear problems, it was decided to use the HLLC approximate Riemann solver which is based on an exact resolution of a Riemann problem using an approximate wave speeds propagation which are unknowns in the original exact Riemann problem.

The main advantages of the HLLC solver are its ability to capture strong shocks without producing spurious oscillations, and of propagating rarefactions in the presence of low-density flow while preserving the entropy condition (see Reference [10]). This, generally, may not be guaranteed by a linearized approximate Riemann solver, which violates the entropy condition and may end up computing rarefaction shocks. This solver also preserves initially positive densities and pressures.

To implement non-reflecting boundary conditions, we use a zonal approach proposed by Freund [11], that combines the techniques proposed by Ta'asan and Nark [12] and Berenger [13]. It consists of adding to the Euler equations advective and damping terms in all directions, but that only become effective in the inflow and outflow zones.

The overall approach used here can still be labelled as a FEM, with the degenerate case of the DGM, corresponding to zeroth order basis functions, being the classical FVM. The approach is seen to contain many of the advantages of the FVM and FEM. First, is the absence of a large global matrix; second, is the higher accuracy given by the FEM basis functions as compared to the discrete gradients required by the FVM; and, third, is the ease of incorporation of slope limiters. Finally, the approach can use uniform or hybrid meshes and is highly parallelizable.

2. DISCRETIZATION DETAILS

Consider the 3D Euler equations in conservative form:

$$\frac{\mathrm{d}}{\mathrm{d}t}Q + \sum_{i=1}^{i=3} \frac{\partial F_i}{\partial x_i} = 0 \quad \text{on } \Omega \times [0, T]$$

$$Q = \begin{bmatrix} \rho \\ \rho u \\ \rho v \\ \rho w \\ E \end{bmatrix}, \quad F_1 = \begin{bmatrix} \rho u \\ \rho u^2 + P \\ \rho uv \\ \rho uw \\ (E+P)u \end{bmatrix}, \quad F_2 = \begin{bmatrix} \rho v \\ \rho uv \\ \rho v^2 + P \\ \rho vw \\ (E+P)v \end{bmatrix}, \quad F_3 = \begin{bmatrix} \rho w \\ \rho uw \\ \rho vw \\ \rho w^2 + P \\ (E+P)w \end{bmatrix} \tag{1}$$

where ρ, u, v, w, E, and P represent density, Cartesian velocity components, total energy per unit volume, and pressure, respectively.

Taking finite element basis function sets that contain polynomials of degree N on each volume T_i such that $\Omega = \bigcup_{i=1}^{i=M} T_i$, the approximate solution is sought in this finite element space denoted by V^N, and is determined from the following weak formulation:

Let $F = (F_1, F_2, F_3)$, and for any $v(x) \in V^N$

$$\frac{\mathrm{d}}{\mathrm{d}t} \int_{T_i} Qv(x)\,\mathrm{d}x + \sum_{j \in N(T_i)} \int_{T_i \cap T_j} F \cdot n_{ij} v(x)\,\mathrm{d}\Gamma - \int_{T_i} F \cdot \nabla v(x)\,\mathrm{d}x = 0 \tag{2}$$

where $N(T_i)$ is the set of neighbours sharing an edge with T_i and n_{ij} is the outward unit normal to $T_i \cap T_j$.

As with a Galerkin scheme, the test functions are chosen to be the local basis functions:

$$v(x) = \varphi_k(x) \quad k = 1, \ldots, L$$

The local basis functions are defined by considering the following oriented tetrahedron

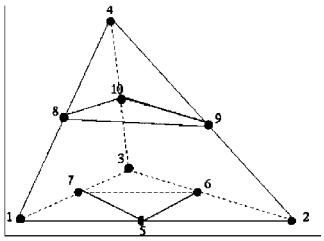

$$\varphi_k = L_k \quad k = 1, 4 \quad \text{for } P^1 \text{ interpolation}$$

while for the P^2 interpolation we take

$$\begin{aligned} \varphi_i &= L_i(2L_i - 1) \quad i = 1, 2, 3, 4 \\ \varphi_i &= 4L_jL_k \quad i = 5, 6, 7, 8, 9, 10 \end{aligned} \tag{3}$$

where j and k are nodes located along the same edge as i and $(L_k,\ k = 1, \ldots, 4)$ are the volume co-ordinates of the tetrahedron.

2.1. Evaluation of the integrals

There are several ways to evaluate these integrals, Atkins and Shu proposed [14] a quadrature-free implementation based on the expansion of the fluxes in a chosen local basis set. This process requires less storage than conventional implementation, however, the accuracy of the flux expansion is not evident in the non-linear case.

Here, the resulting integrals are evaluated by Gauss quadrature rules, which are exact, with p Gaussian points, for polynomials of degree $(2p - 1)$.

This method is uniformly $(N + 1)$th order accurate when polynomials of degree N are used [15, 16], which leads to a high-order method.

For the interface integral:

$$\int_{T_i \cap T_j} F \cdot n_{ij} \varphi_k(x)\, \mathrm{d}\Gamma \quad k = 1, \ldots, 4 \tag{4}$$

one can approach the flux $F \cdot n_{ij}$ by a numerical flux chosen in various manners. An approximate resolution of a Riemann problem at the interfaces between the volume of integration, put forward by Toro *et al.* [17], and known as the HLLC Riemann solver, is proposed here.

Let us denote Φ_{ij} this flux by

$$\Phi_{ij} \sim F \cdot n_{ij} \tag{5}$$

then, an appropriate quadrature rule is used to calculate the integrals:

$$\int_{T_i \cap T_j} \Phi_{ij} \varphi_k(x)\, \mathrm{d}\Gamma \quad k = 1, \ldots, 4 \tag{6}$$

2.2. The HLLC solver

In order to capture contact discontinuities and shocks, the HLLC Riemann solver (see details in Reference [18]) is used to compute the numerical fluxes. This scheme is a modification of the HLL [12] scheme. The central idea is to assume a wave configuration for the solution that consists of three waves separating four constant states. In the Euler equations, the solution of the Riemann problem consists of a contact wave and two acoustic waves, which may be either shocks or expansion fans.

This solver is based on Godunov's method where the approximate solutions are constructed by averaging intermediate states in the exact solution, respecting certain principles like exactly resolving isolated shocks and contact discontinuities.

The three-dimensional Euler flux in the normal direction is given by $F \cdot n_{ij}$, where

$$F \cdot n_{ij} = \begin{bmatrix} \rho q \\ \rho u q + P n_{ij}^x \\ \rho v q + P n_{ij}^y \\ \rho w q + P n_{ij}^z \\ (E + P) q \end{bmatrix}, \quad n_{ij} = \begin{bmatrix} n_{ij}^x \\ n_{ij}^y \\ n_{ij}^z \end{bmatrix}, \quad q = u n_{ij}^x + v n_{ij}^y + w n_{ij}^z \tag{7}$$

q is the component of velocity acting in the normal direction. Therefore, one can resolve a Riemann problem in the normal direction and the problem becomes one-dimensional.

The four states, from left to right are denoted by $Q_\mathrm{L}, Q_\mathrm{L}^*, Q_\mathrm{R}^*$, and Q_R and are separated by the wave speeds S_L, S_M and S_R, respectively. S_M is the contact wave speed and S_L and S_R are the left acoustic wave speed and the right acoustic wave speed, respectively.

If the flow is supersonic, then the flux is given either by $F(Q_\mathrm{L})$ if $S_\mathrm{L} > 0$, which corresponds to a supersonic flow from left to right, or by $F(Q_\mathrm{R})$ if $S_\mathrm{R} < 0$, which corresponds to a supersonic flow from right to left.

In the more complex subsonic case, when $S_\mathrm{L} < 0 < S_\mathrm{R}$, we consider two intermediate states, between the two acoustic waves, separated by a contact discontinuity.

The HLLC solver proposed is based on an exact resolution of a Riemann problem, while averaging the wave speeds $S_\mathrm{L}, S_\mathrm{M}$, and S_R in an appropriate manner.

By applying the Rankine–Hugoniot conditions across each of the waves of speeds S_L, S_M, and S_R, the HLLC flux is obtained for the approximate Godunov scheme as follows:

$$\text{flux} = \begin{cases} F(Q_L) & \text{if } S_L > 0 \\ F(Q_L) + S_L(Q_L^* - Q_L) & \text{if } S_L \leqslant 0 < S_M \\ F(Q_R) + S_R(Q_R^* - Q_R) & \text{if } S_M \leqslant 0 \leqslant S_R \\ F(Q_R) & \text{if } S_R < 0 \end{cases} \tag{8}$$

Acoustic wave speeds estimates chosen in this solver are extremely robust and yield the exact velocity for isolated shocks. The algorithm can be found in Reference [20].

2.3. Time integration

We obtain, after space discretization, the following ODE:

$$\frac{\mathrm{d}}{\mathrm{d}t} Q = L(Q,t) \tag{9}$$

$L(Q,t)$ is the approximation of $\sum_{i=1}^{i=3} \partial F_i/\partial x_i$ by the DGM described above.

The solution is advanced in time with a TVD Runge–Kutta method, with p stages

$$\begin{aligned} Q^0 &= Q^n \\ Q^l &= \sum_{e=0}^{e=l-1} [\alpha_{le} Q^e + \beta_{le} \Delta t L(Q^e, t^n + d_l \Delta t)], \quad l = 1, 2, \ldots, p \\ Q^{n+1} &= Q^p \end{aligned} \tag{10}$$

Here, the coefficients p, α, β and d are related to the order and stability of the scheme.

2.4. The generalized slope limiter

The slope limiter used in this code is inspired from the modified slope limiter of Cockburn and Shu [14]. This limiter maintains the formal accuracy of the scheme at extrema and is formally uniformly second order in space and time.

This generalized slope limiter named $\Lambda\Pi$ is a non-linear projection operator and is devised in such a way that if $Q' = \Lambda\Pi U$ for some function U, then the mapping

$$Q^l \to \omega^{il} \quad \text{with } \omega^{il} = Q^l + \frac{\beta_{il}}{\alpha il} \Delta t L(Q^l) \tag{11}$$

is stable, that is, $|\omega^{il}| \leqslant Q^l$.

The above time discretization algorithm (Equation (10)) is then modified as follows:

$$\begin{aligned} Q^0 &= \Lambda\Pi Q^n \\ Q^l &= \Lambda\Pi \left(\sum_{e=0}^{e=l-1} [\alpha_{le} Q^e + \beta_{le} \Delta t L(Q^e, t^n + d_l \Delta t)] \right), \quad l = 1, 2, \ldots, p \\ Q^{n+1} &= Q^p \end{aligned} \tag{12}$$

The use of the generalized slope limiter is crucial to ensure the stability of the method when shocks are present. It is redundant when the solution is smooth.

When piecewise constant approximations are used for the space discretization and the first-order scheme is employed for time discretization, a standard FVM is obtained and the slope limiter becomes the identity.

2.5. *Non-reflecting boundary conditions*

It was observed in Colonius *et al.*'s work [21] that reflection errors are induced when linearized boundary conditions are used for non-linear equations such as the Euler equations. In cases where high amplitude non-linear waves must exit the domain without significant reflections, it has been found necessary to add non-physical exit zones, known as buffer zones, to the computation.

Several authors have proposed techniques to minimize reflections. Ta'asan and Nark [22] add a convective term to the linear Euler equations to force them to be supersonic at the borders of the numerical domain. Berenger [23] proposed another zonal boundary treatment for Maxwell's equations by adding a damping term to the equations. Hu [24] extended this technique to the linear Euler equations.

Here, we propose a zonal approach used by Freund [25] that combines the techniques proposed by Ta'asan, Nark and Berenger. It adds to the Euler equations advective and damping terms in all directions that only become effective in the inflow and outflow zones.

Suppose that x_1 is the streamwise direction of the wave, the modified equations can be written as

$$\frac{\mathrm{d}}{\mathrm{d}t} Q + \sum_{i=1}^{i=3} \frac{\partial F_i}{\partial x_i} = -\sigma(x_1)[Q - Q_{\text{target}}] - U_{\text{c}}(x_1)\frac{\partial Q}{\partial x_1} \tag{13}$$

where $\sigma(x_1)$ is an artificial damping function and $U_{\text{c}}(x_1)$ is an artificial convection velocity.

The form chosen for these functions is given by

$$\sigma(x) = \begin{cases} \sigma_{0l}\left(\dfrac{w_l - x}{w_l}\right)^{\beta_{\sigma l}} & 0 \leqslant x < w_l \\ 0 & w_l \leqslant x < x_{\max} - w_r \\ \sigma_{0l}\left(\dfrac{x - (x_{\max} - w_r)}{w_r}\right)^{\beta_{\sigma r}} & x_{\max} - w_r \leqslant x \leqslant x_{\max} \end{cases} \tag{14}$$

$$U_{\text{c}}(x) = \begin{cases} U_{0l}\left(\dfrac{w_l - x}{w_l}\right)^{\beta_{ul}} & 0 \leqslant x < w_l \\ 0 & w_l \leqslant x < x_{\max} - w_r \\ U_{0l}\left(\dfrac{x - (x_{\max} - w_r)}{w_r}\right)^{\beta_{ur}} & x_{\max} - w_r \leqslant x \leqslant x_{\max} \end{cases} \tag{15}$$

where $\sigma_{0(l,r)}$, $U_{0(l,r)}$ are the maximum values of the damping and convective terms at the left and right domain edges, and w_l, w_r are the widths of the support of σ and U. $U_{0(l,F)}$ is taken to be greater than the sound speed.

Some of the advantages of this technique are its robustness and that non-linear reflection errors from the far-field boundary are minimized. It should also be noted that no additional equation, but only additional terms, are generated and hence no extra variables need be stored. Finally, it has been proven that this technique is appropriate to non-linear calculations (see Reference [25]).

2.6. Summary of the problem to resolve

Here we recall the problem to resolve and the method used for the numerical resolution. The continuous problem is given by the following formulation:

$$\frac{\mathrm{d}}{\mathrm{d}t}Q+\sum_{i=1}^{i=3}\frac{\partial F_i}{\partial x_i}=-\sigma(x_1)[Q-Q_{\text{target}}]-U_{\mathrm{c}}(x_1)\frac{\partial Q}{\partial x_1}\quad \text{on } \Omega\times[0,T] \tag{$*$}$$

$$\sigma(x)=\begin{cases}\sigma_{0l}\left(\dfrac{w_l-x}{w_l}\right)^{\beta_{\sigma l}} & 0\leqslant x<w_l\\ 0 & w_l\leqslant x<x_{\max}-w_r\\ \sigma_{0l}\left(\dfrac{x-(x_{\max}-w_r)}{w_r}\right)^{\beta_{\sigma r}} & x_{\max}-w_r\leqslant x\leqslant x_{\max}\end{cases}$$

$$U_{\mathrm{c}}(x)=\begin{cases}U_{0l}\left(\dfrac{w_l-x}{w_l}\right)^{\beta_{ul}} & 0\leqslant x<w_l\\ 0 & w_l\leqslant x<x_{\max}-w_r\\ U_{0l}\left(\dfrac{x-(x_{\max}-w_r)}{w_r}\right)^{\beta_{ur}} & x_{\max}-w_r\leqslant x\leqslant x_{\max}\end{cases}$$

In Equation ($*$), the left terms are the Euler equations and the right terms contain the damping and the advective terms used for the non-reflecting boundary conditions.

For the numerical discretization, we use a Runge–Kutta scheme for the time evolution and for space discretization we choose a discontinuous Galerkin method with the HLLC solver to compute the numerical fluxes. These fluxes are given by the following formulation:

$$\text{flux}=\begin{cases}F(Q_{\mathrm{L}}) & \text{if } S_{\mathrm{L}}>0\\ F(Q_{\mathrm{L}})+S_{\mathrm{L}}(Q_{\mathrm{L}}^{*}-Q_{\mathrm{L}}) & \text{if } S_{\mathrm{L}}\leqslant 0<S_{\mathrm{M}}\\ F(Q_{\mathrm{R}})+S_{\mathrm{R}}(Q_{\mathrm{R}}^{*}-Q_{\mathrm{R}}) & \text{if } S_{\mathrm{M}}\leqslant 0\leqslant S_{\mathrm{R}}\\ F(Q_{\mathrm{R}}) & \text{if } S_{\mathrm{R}}<0\end{cases}$$

where S_{L}, S_{M} and S_{R} are the three wave speeds from left to right and Q_{L}, Q_{L}^{*}, Q_{R}^{*}, and Q_{R} are the four states separated by the wave speeds.

To ensure the stability of the numerical method, a non-linear slope limiter is used such as the accuracy is maintained.

3. NUMERICAL ASSESSMENT AND RESULTS

We give here some numerical results obtained via DGM to demonstrate its performance and robustness. Non-linear discontinuities (shocks), rarefactions and acoustic pulses are resolved by a second-order method.

3.1. Shock waves

The problem consists of a tube, with a membrane located at $x = x_0$, separating two gases of different pressures and densities.

The initial states to the left and right of the diaphragm are given by

$$Q(x, y, z, 0) = \begin{cases} Q_l & x < x_0 \\ Q_r & x \geqslant x_0 \end{cases}$$

where

Test	ρ_L	U_L	P_L	ρ_R	U_R	P_R
1	1.0	0.75	1.0	0.125	0.0	0.1

This test is denoted as the Sod test problem and the solution consists of a left rarefaction, a right contact discontinuity and shock.

The specific internal energy is given by: $\textit{Internal energy} = P/(\gamma - 1)\rho$.

Here, in Figures 1 and 2, we compare the solution obtained from the HLLC solver with a solution obtained by the Roe scheme.

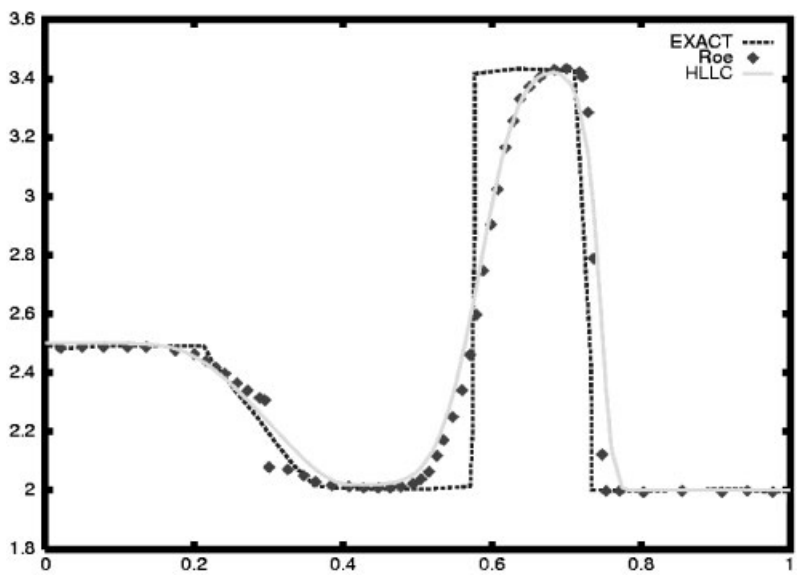

Figure 1. Shock-collision, internal energy comparison, $x_0 = 0.3$, solution at time $t = 0.2$ units.

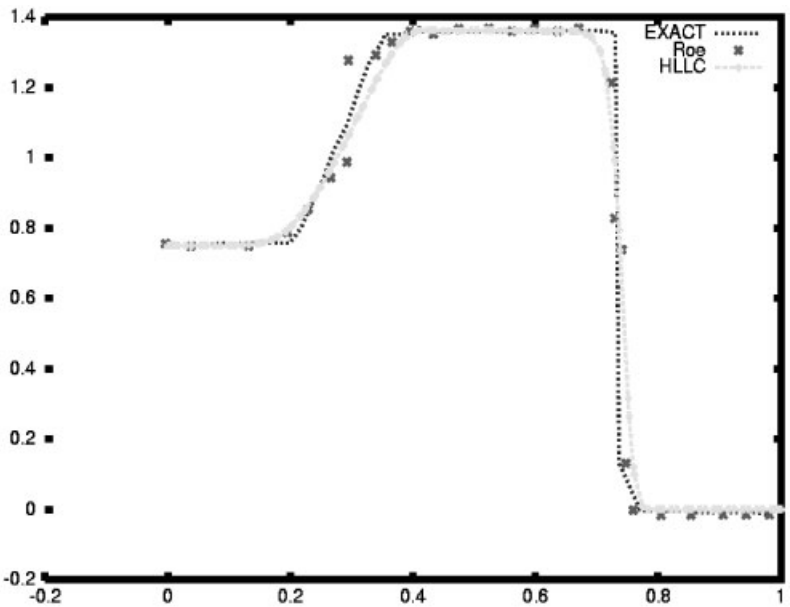

Figure 2. Shock-collision, velocity comparisons, $x_0 = 0.3$, solution at time $t = 0.2$ units.

The grid used for this test corresponds to 43 points in the x-direction where $0 \leqslant x \leqslant 1$ for the HLLC solver and 100 points for the Roe solver.

We can note that the solutions obtained from the Roe solver are not quite correct near the sonic point, but that the HLLC solutions are very accurate near these sonic points.

3.2. Transonic flow over a NACA0012

We present next a numerical experiment with an airfoil to show the shock capturing capability of the method, even on coarse grids.

The test consists of a transonic flow around a NACA0012 at Mach 0.85. A shock appears at the 75% chord location.

In this test, the mesh has only 9729 nodes, for a non-dimensional characteristic length of 1 and a total domain length of 12 (Plate 1).

Figures 3 and 4 represent both lower and upper profiles of the Mach number and the pressure, respectively.

Although the grid is intentionally chosen to be quite asymmetric, Figures 3 and 4 show the solutions to be perfectly symmetric.

In addition, if we compare the solution to the one obtained with a refine grid in Figure 5, one can note the acceptable quality of the transonic results obtained with a very coarse grid.

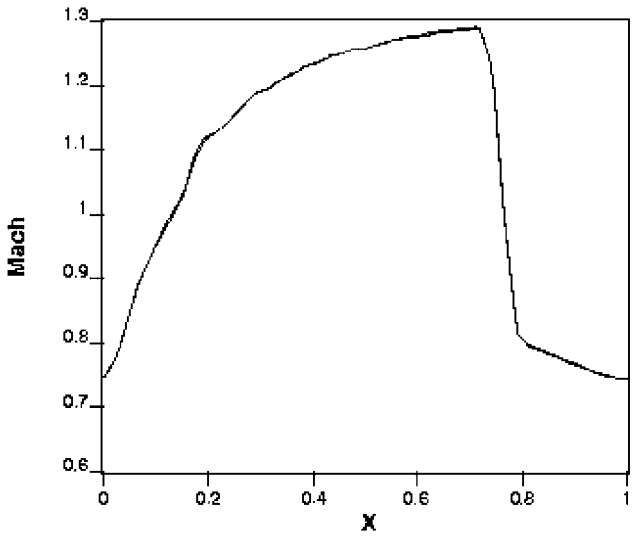

Figure 3. Mach number, NACA0012 wing, Mach = 0.85, AoA = zero.

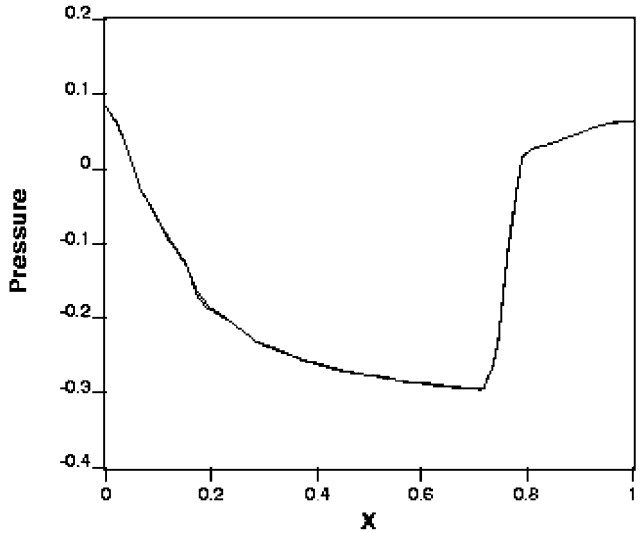

Figure 4. Pressure, NACA0012 wing, Mach = 0.85, AoA = zero.

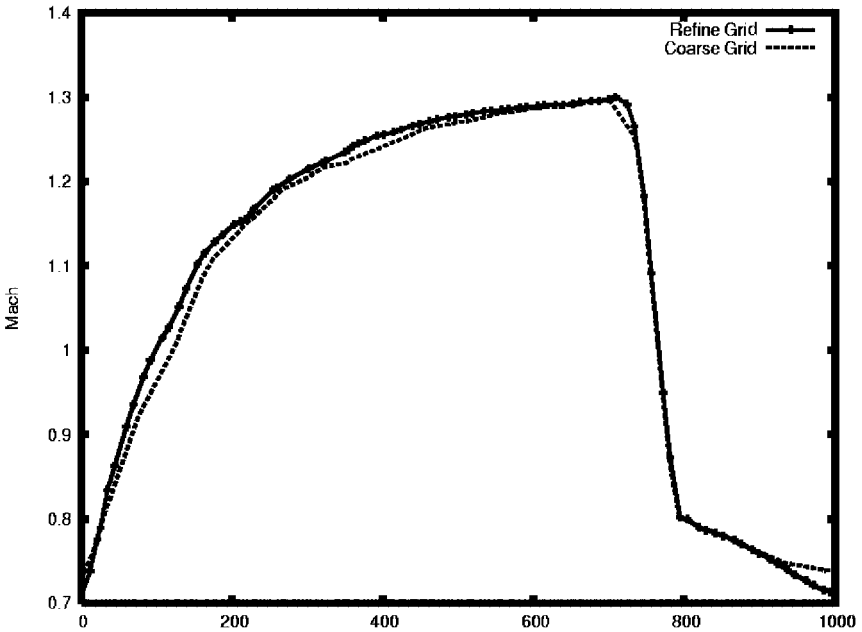

Figure 5. Mach Comparison, NACA0012 wing, Mach = 0.85, AoA = zero.

3.3. Aero-acoustics application

The unsteady flow is initialized by a Gaussian disturbance with a half-width of 3 as follows:

$$\begin{bmatrix} \rho \\ U \\ V \\ w \\ P \end{bmatrix} = \begin{bmatrix} \rho_\infty + 0.01 \exp(-\ln(2)\dfrac{(x^2+y^2)}{9} \\ 0.0 \\ 0.0 \\ 0.0 \\ P_\infty + 0.01 \exp(-\ln(2)\dfrac{(x^2+y^2)}{9} \end{bmatrix}$$

The computational domain is $(x, y, z) \in [-50, 50] \times [-50, 50] \times [0, 20]$, and the number of points is around $32 \times 32 \times 12$ in the three directions.

The disturbance pulses are relatively small so that the non-linear numerical solutions may be compared with the solution of the linearized Euler equations. Plate 2and Figure 6 represent the 2D acoustic pressure and the acoustic pressure along $y = 0$, respectively, compared to the exact solution. The high quality of the numerical solution is apparent.

3.4. Non-reflecting boundary evaluation

To test the effect of the damping technique, we consider the above experiment of acoustic pulse propagation and compare the result with the one obtained without damping terms when the

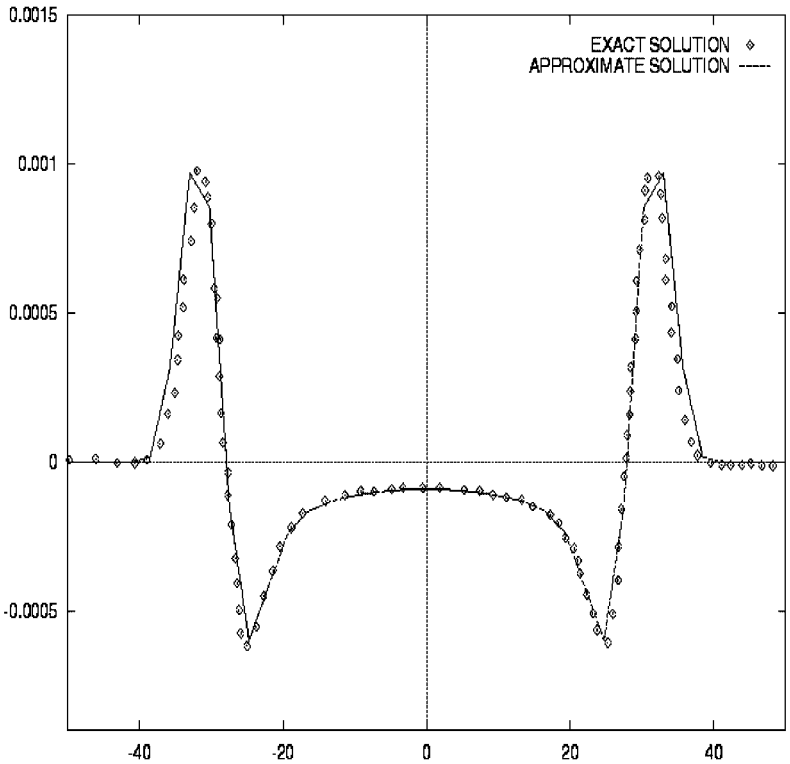

Figure 6. Acoustic pressure along $y = 0$, time $= 30$ units.

pulse leaves the domain. It was observed that the power coefficient β fixed to 3 is numerically optimal in such test case.

The solutions given by Plates 3 and 4 demonstrate the efficiency of the absorbing layer. We have also compared the pressure along $y = 0$ as is shown in Figure 7. Comparisons at different times with damping layer and with same coefficients to show the efficiency of the damping method when the wave continues to leave the domain is presented in Figure 8. These tests show the efficiency of the non-reflecting boundary technique used in the present methodology.

3.5. Mesh convergence

We study in this section the mesh convergence for DGM method in resolving acoustic problems.

First we recall the definition of the grid convergence index (GCI) proposed by Roache in his book [26]. The idea is to give an error estimator which is derived from the theory of generalized Richardson extrapolation:

$$F_{\text{exact}} = F_1 + \frac{(F_1 - F_2)}{(r^p - 1)}$$

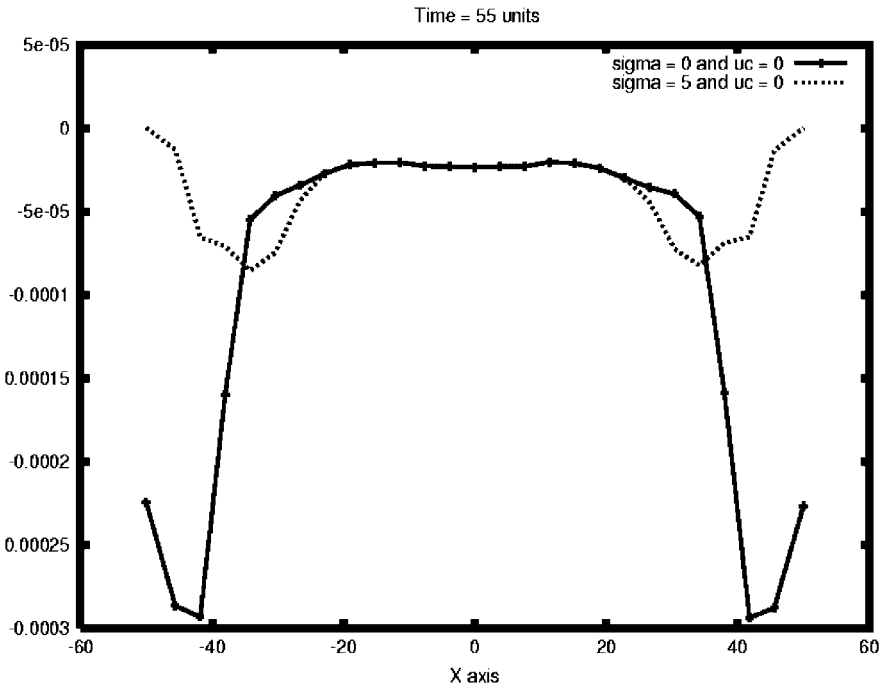

Figure 7. Pressure comparison along $y = 0$, time $= 55$ units.

where F_1 is a fine grid solution and F_2 is a coarse grid solution, r is the value of the grid ratio and p is the order of the numerical method.

We define the Estimated fractional error E_1 for the fine grid solution F_1 as

$$E_1 = \frac{\varepsilon}{(r^p - 1)}$$

$$\varepsilon = \frac{(F_1 - F_2)}{F_1}$$

The relative error grid convergence index (GCI) for the fine grid is then given by

$$\mathrm{GCI}_1 = \frac{3|\varepsilon|}{(r^p - 1)}$$

And the relative error grid convergence index for the coarse grid is then given by

$$\mathrm{GCI}_2 = \frac{r^p 3|\varepsilon|}{(r^p - 1)}$$

In Table I we present, the GCI for fine and coarse grids taking $r = 2$. The first and second interpolations are considered.

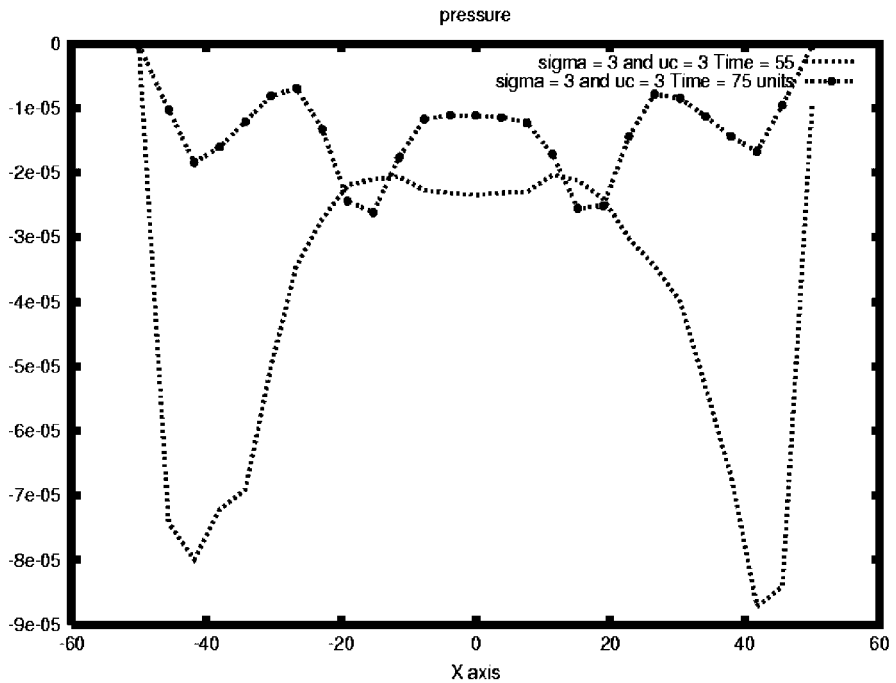

Figure 8. Pressure comparison at different times with width = 7.

Table I. GCI for the acoustic problem.

Fine grid		Coarse grid	
Method's order	GCI	Method's order	GCI
1	3.45%	1	6.90%
2	2.41%	2	4.84%

4. CONCLUSIONS

It can be deduced from the numerical results presented here that the DGM is well suited for propagating shocks, even on coarse grids, and for accurately treating rarefactions near low-density flow, features that cannot be guaranteed by a linearized approximate Riemann solver. Owing to its accuracy and to the HLLC Riemann solver, this approach has high potential for solving strong discontinuities in the aerodynamic and aero-acoustic areas.

REFERENCES

1. Reed WH, Hill TR. Triangular Mesh Methods for the Neutron Transport Equations. *Los Alamos Scientific Laboratory Report LA-UR-73-479*, 1973.
2. Cockburn B, Shu CW. The Runge-Kutta discontinuous Galerkin method for time-conservation laws V, multidimensional systems. *Journal of Computational Physics* 1998; **141**:199–224.

3. Bassi F, Rebay S. Numerical evaluation of two discontinuous Galerkin methods for the compressible Navier–Stokes equations. *International Journal for Numerical Methods in Fluids* 2002; **40**:197–207.
4. Remaki M, Fezoui L. Une méthode Galerkin Discontinu pour la résolution des équations de Maxwell en milieu hétérogène. INRIA research report no 3501, 1998.
5. Remaki M, Fezoui L. Comparison between two time-domain methods. *Conference Proceedings*, *15th Annual Review of Progress in Applied Computational Electromagnetics at the Naval Postgraduate School*, vol. 1. March 15–20. Monterey, CA, USA, 1999; 608–614.
6. Karniadakis GE, Sherwin SJ. *Spectral/hp Element Methods in CFD.* Oxford University Press: Oxford, 1999.
7. Warburton TC. Spectral/hp methods on polymorphic multi-domain: Algorithms and applications. *Ph.D. Thesis*, Brown University, 1998.
8. Cockburn B, Karniadakis GE, Shu CW. *Discontinuous Galerkin Methods*: *Computation and Application*. Springer: Berlin, 2000.
9. Toro EF. *Riemann Solvers and Numerical Methods for Fluid Dynamics. A Practical Introduction* (2nd edn). Springer: Berlin, 1999.
10. Remaki M, Habashi WG, Ait-Ali-Yahia D, Jay A. A Discontinuous Galerkin method for Multiple Pure Tone Noise in Gas Turbines. *The 40th AIAA Aerospace Science Meeting and Exhibit 14–17*, Reno, USA, 2002.
11. Freund B. A proposed inflow/outflow boundary condition for direct computation of aerodynamic sound. Stanford University, Department of Mechanical Engineering, 1998.
12. Ta'asan S, Nark DM. An absorbing buffer zone technique for acoustic wave propagation. *AIAA paper* 95-0146, 1995.
13. Berenger JB. A perfectly matched layer for the absorption of electromagnetic waves. *Journal of Computational Physics* 1994; **114**:185–200.
14. Atkins HL, Shu CW. Quadrature-free implementation of discontinuous Galerkin methods for hyperbolic equations. *AIAA Journal* 1998; **36**:775–782.
15. Cockburn B, Shu CW. The Runge-Kutta local P^1-Discontinuous-Galerkin Finite Element Method for Scalar Conservation Laws. IMA Preprint Series 388, University of Minnesota, 1988.
16. Chavent G, Cockburn B. The Local Projection P^0P^1-Discontinuous-Galerkin Finite Element Method for Scalar Conservation Laws. IMA Preprint Series 341, University of Minnesota, 1987.
17. Toro EF, Spruce M, Speares W. Restoration of the Contact Surface in the HLL-Riemann Solver. *Shock Waves* 1994; **4**:25–34.
18. Toro EF. *Riemann Solvers and Numerical Methods for Fluid Dynamics*, *A Practical Introduction* (2nd edn). Springer: Berlin, 1999.
19. Harten A, Lax PD, Van Leer B. On upstream differencing and Godunov type schemes for hyperbolic conservation laws. *SIAM Review* 1983; **25**(1):35–61.
20. Batten P, Clarke N, Lambert C, Causon DM. On the choice of wave speeds for the HLLC Riemann solver. *SIAM Journal on Scientific Computing* 1997; **18**(6):1553–1570.
21. Colonius T, Lele SK, Moin P. Boundary conditions for direct computation of aerodynamic sound generation. *AIAA Journal* 1993; **31**:1574–1582.
22. Ta'asan S, Nark DM. An absorbing buffer zone technique for acoustic wave propagation. *AIAA Paper 95-0146*, 1995.
23. Berenger JP. A perfectly matched layer for the absorption of electromagnetic waves. *Journal of Computational Physics* 1994; **114**:185–200.
24. Hu FQ. On absorbing boundary conditions for linearized euler equations by a perfectly matched layer. *ICASE Report 95-70*, NASA Langley, 1995.
25. Freund JB. *A Proposed Inflow/Outflow Boundary Condition for Direct Computation of Aerodynamic Sound.* Stanford University, Department of Mechanical Engineering, 1998.
26. Roache PJ. *Fundamentals of Computational Fluid Dynamics*. Hermosa Publishers: Albuquerque, NM, 1998.

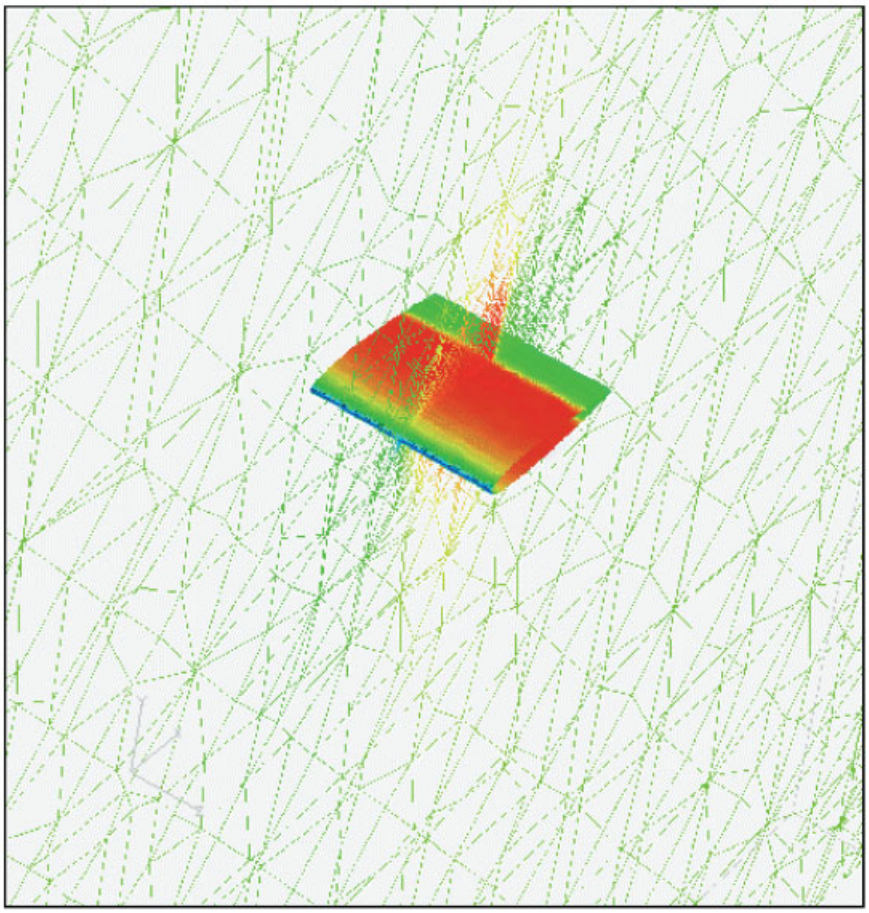

Plate 1. NACA0012 wing mesh and Mach contours.

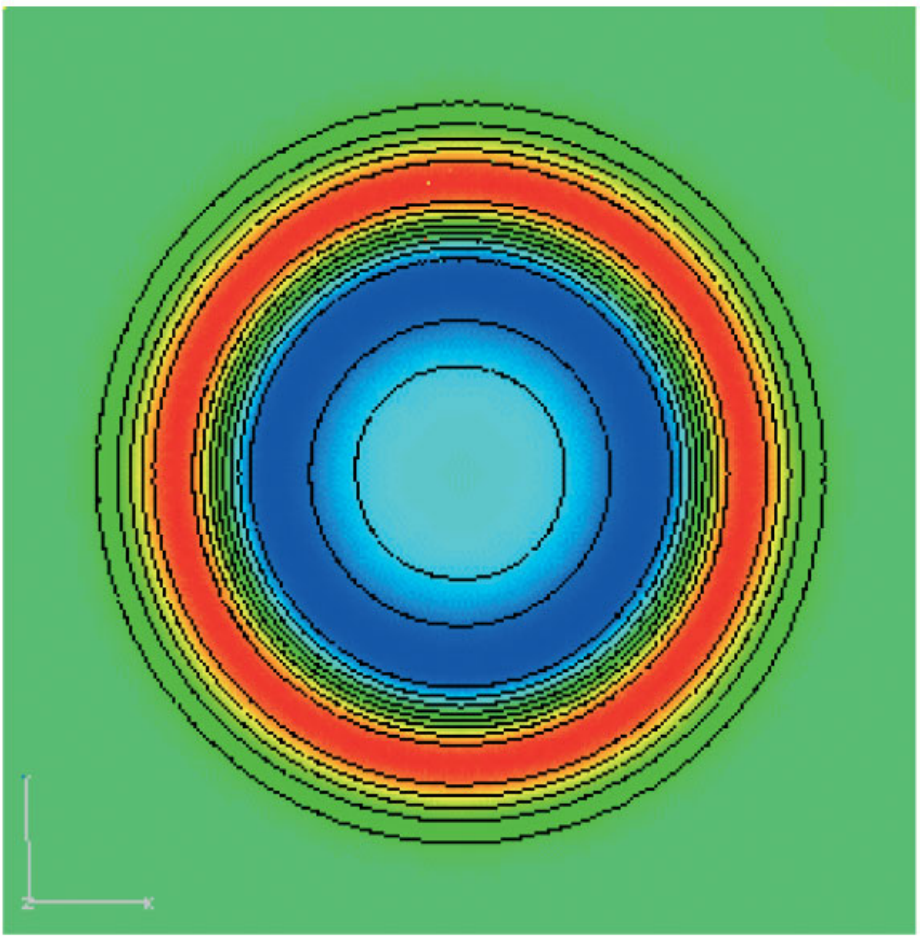

Plate 2. 2D acoustic pressure, time = 30 units.

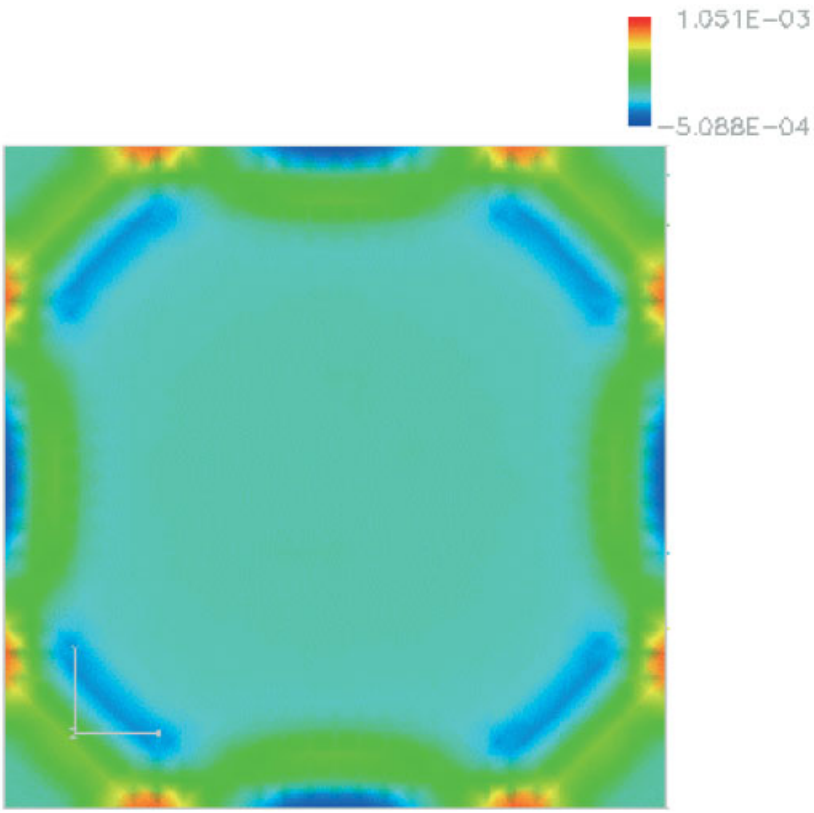

Plate 3. Solution with no damping, time = 55 units.

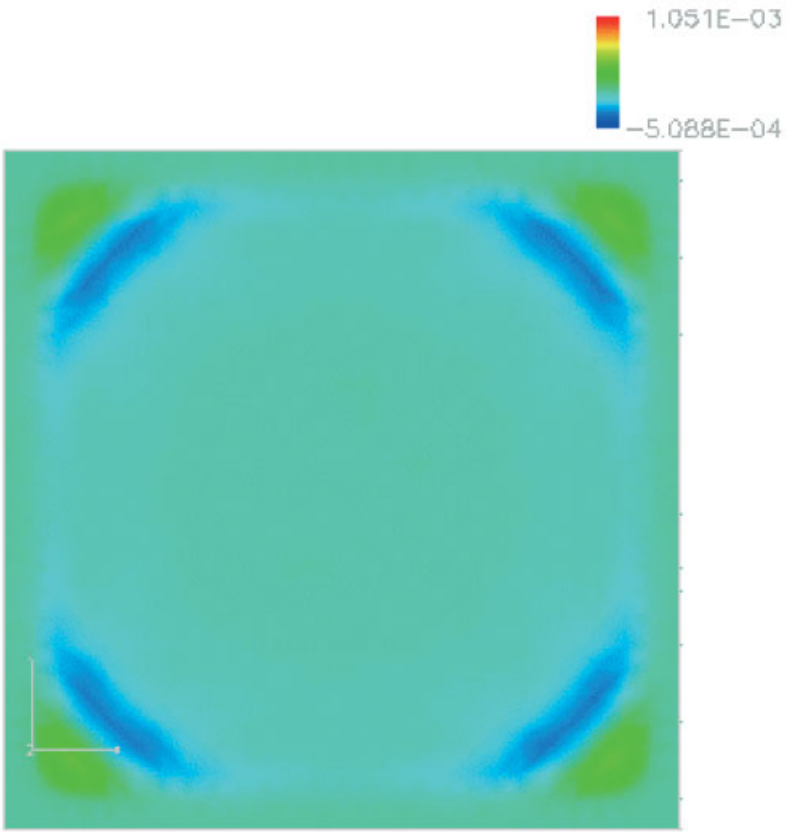

Plate 4. Solution with damping, time = 55 units.